



Study on the Preparation and Properties of a Co-Based Barrier Layer by Diffusion Welding

Shangwei Jiang^{1,2,3} · Zhixiang Kuang^{1,2,3} · Xiaoming Hu^{1,2,3} · Xin Chen^{1,2,3} · Fuxiang Zou^{1,2,3} · Xi'an Fan^{1,2,3,4} 

Received: 14 May 2023 / Accepted: 18 December 2023 / Published online: 22 January 2024
© The Minerals, Metals & Materials Society 2024

Abstract

In order to improve the stability of Bi_2Te_3 -based thermoelectric devices, we attempted to prepare a barrier layer via diffusion welding using Co powder as the barrier materials. The diffusion welding process was conducted at 674 K for a duration of 5 min. The optimal connection was achieved at the interfaces of $\text{Co}/\text{Bi}_{0.4}\text{Sb}_{1.6}\text{Te}_3$ and $\text{Co}/\text{Bi}_2\text{Te}_{2.7}\text{Se}_{0.3}$. The results showed that the $\text{Co}/\text{Bi}_{0.4}\text{Sb}_{1.6}\text{Te}_3$ joint had diffusion thickness of 1.6 μm , contact resistivity of 0.83 $\mu\Omega\text{ cm}^2$, and bonding strength of 4.86 MPa for the barrier layer. Similarly, the $\text{Co}/\text{Bi}_2\text{Te}_{2.7}\text{Se}_{0.3}$ joint had diffusion thickness of 1.6 μm , contact resistivity of 0.75 $\mu\Omega\text{ cm}^2$, and bonding strength of 3.99 MPa for the barrier layer. The thermoelectric device fabricated through this process exhibited a hot–cold cycle number of 35,000, which was significantly higher than the device with a Ni-based barrier layer under similar experimental conditions. Thus, it indicates that Co is a promising material for the preparation of barrier layers in Bi_2Te_3 -based thermoelectric devices.

Keywords Bi_2Te_3 -based thermoelectric devices · barrier layer · diffusion welding · spark plasma sintering · Co

Introduction

The commercialization of Bi_2Te_3 -based thermoelectric materials on a large scale has made it a popular choice in the field of thermoelectric devices.^{1–6} The encapsulation process of these devices involves connecting the electrode and the thermoelectric materials using soldering or brazing techniques.⁷ However, the poor wetting performance between thermoelectric materials and solders calls for a metallization

treatment to be performed on the two end surfaces of the Bi_2Te_3 -based thermoelectric arm before welding. Ni, with good soldering performance, is often utilized as the metallization layer.⁸ However, thermoelectric devices with Ni-based metallization layers usually failed during the service process.

One of the significant contributors to the failure is the insufficient interface bonding strength of the layers between Ni- and Bi_2Te_3 -based elements.^{9,10} At the contact interface between Ni and Bi_2Te_3 , a NiTe intermetallic compound (IMC) is formed by reaction during use. However, the mechanical properties of this IMC are poor, and the thickness of the reaction layer at the interface increases with the use of the device, which reduces the bonding strength at the interface and ultimately leads to device failure.¹¹ In particular, in $n\text{-Bi}_2\text{Te}_3$, the continuous generation of NiTe IMC leads to the formation of Te-deficient regions close to the interface in the bismuth telluride base material, and the $p\text{-Bi}_2\text{Te}_3$ phase may even appear. This phenomenon seriously affects the thermoelectric properties of such devices.¹² Joints prepared through methods such as magnetic sputtering, electrodeposition, and electroplating have an interface bonding strength of around 8–10 MPa.¹³ However, the temperature difference between the cold and hot surfaces on thermoelectric generators is much higher than that on

✉ Xi'an Fan
groupfxa@163.com

¹ The State Key Laboratory of Refractories and Metallurgy, Wuhan University of Science and Technology, Wuhan 430081, China

² National-Provincial Joint Engineering Research Center of High Temperature Materials and Lining Technology, Wuhan University of Science and Technology, Wuhan 430081, China

³ Key Laboratory for Ferrous Metallurgy and Resources Utilization of Ministry of Education, Wuhan University of Science and Technology, Wuhan 430081, China

⁴ School of Materials and Metallurgy, Wuhan University of Science and Technology, 947 Heping Road, Qingshan District, P. O. Box 185#, Wuhan 430081, People's Republic of China

refrigeration devices, leading to a corresponding increase in interface thermal stress.^{14,15} Therefore, extending the service life of thermoelectric devices can be achieved through two approaches: either by improving the interfacial bonding of Ni/Bi₂Te₃ through process improvement, or by changing the barrier layer material to minimize interfacial reactions and the formation of IMCs that could potentially compromise interfacial stability.

Liu et al.¹⁶ aimed to improve the Ni/Bi₂Te₃ interface connection by directly sintering Ni powder onto the end surface through powder metallurgy. The resulting Ni/Bi₂Te₃ interface bonding strength was found to be 20–30 MPa, which is enough to withstand the cold and hot cycle experiments of the Bi₂Te₃ hot surface at room temperature and above 473 K. However, the contact resistivity of Ni/Bi₂Te_{2.7}Se_{0.3} (210 μΩ cm²) was increased 40-fold compared to samples prepared through traditional electrodeposition methods (~5 μΩ cm²), due to the formation of NiTe IMCs, voids and defects. Hsieh et al.¹⁷ utilized a chemical deposition method to deposit a Co-P layer on *n*-PbTe, and discovered that the Co-P layer was more effective in preventing element diffusion than the Ni-P layer. Similarly, Wang et al.¹⁸ employed electroplating to deposit a Co-P layer on *n*-Bi₂Te₃ and found that the Co-P layer significantly improved the strength of both *n*-Bi₂Te₃ and *p*-Bi₂Te₃, increasing the former 1.5-fold and the latter sevenfold. Additionally, the fracture mode of the samples became more ductile with the addition of the Co-P layer. Despite these promising results, however, the methods for depositing the Co-P layer, such as chemical plating and electroplating, are complex and oversensitive and can cause environmental pollution. The P content in the coating also has a substantial effect on its performance, and uniformity of the coating can be compromised if the plating solution is not regularly replenished. The current challenge is how to develop a simple, stable and environmentally friendly method for preparing a Co-based barrier layer.

In this work, a Co-based diffusion barrier was prepared by diffusion welding the Co powder into Bi₂Te₃-based thermoelectric materials. The microstructure, contact resistivity, mechanical strength, and performance of Co powder/Bi₂Te₃-based materials were investigated under various temperatures and time during diffusion bonding. Additionally, the stability of the diffusion barrier also studied during service.

Experimental Section

The *p*-type Bi_{0.4}Sb_{1.6}Te₃ and *n*-type Bi₂Te_{2.7}Se_{0.3} substrates with dimensions of φ30 mm × 1.6 mm purchased from Hubei Sagreon New Energy Technology Co., Ltd. were polished to remove surface scratches and oxide layers, then cleaned with acetone to remove surface stains. The polished and cleaned substrates were placed in a graphite mold (φ30 mm) along

with the weighed Co powder, and diffusion welding was implemented by the spark plasma sintering method. The sintering conditions for diffusion welding were as follows: argon atmosphere, uniaxial pressure of 60 MPa, heating rate of 40 K min⁻¹, sintering temperatures of 673 K, 723 K, and 773 K, and holding times of 5 min and 10 min, with a cooling rate of 5 K min⁻¹. Lastly, *n*-type and *p*-type bismuth telluride-based substrates with a Co barrier layer were prepared, and the thermoelectric devices based on the Co-based diffusion barrier were fabricated.

Characterization

The interface morphology and element distribution were observed by a field-emission scanning electron microscope (SEM, Nova 400 NanoSEM, FEI, USA) and an energy-dispersive spectrometer (EDS, IE 350Penta FET-3, Oxford, UK). The contact resistivity of the thermoelectric joints was measured using a contact resistivity tester provided by Shenzhen Advanced Electronic Materials International Innovation Research Institute. The device principle is depicted in Fig. 1. In the setup, probes 1 and 4 function as current probes, while probes 2 and 3 act as voltage probes. Probes 1, 2, and 4 remain stationary, and only probe 3 is able to move horizontally. By applying a fixed current *I* to probes 1 and 4, the movement of probe 3 leads to a sudden voltage change *V_c* at the interface between the Bi₂Te₃ and the Co layer. The interfacial contact resistivity can be determined using Eq 1:

$$\rho = \frac{V_c}{I} \cdot A \quad (1)$$

where *A* is the contact area of the interface. The interfacial bonding strength was measured using the HP-100 Digital Push-Pull Gauge (HANDPI Instruments Ltd.). The service performance of the thermoelectric devices was tested by an alternating current impact testing machine.

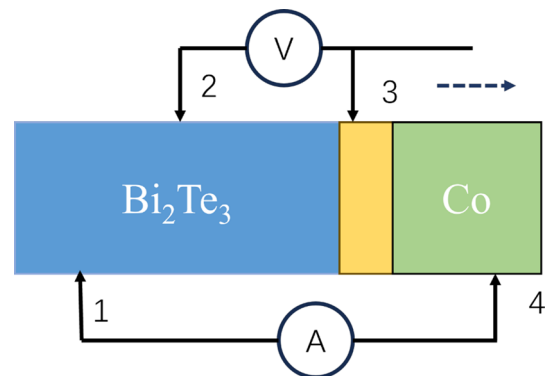


Fig. 1 Schematic diagram of interface contact resistivity test principle.

Results and Discussion

Figure 2 displays the SEM and EDS results of the Co/Bi_{0.4}Sb_{1.6}Te₃ joints fabricated under different diffusion bonding conditions. The results indicate that the interface of Co/Bi_{0.4}Sb_{1.6}Te₃ exhibits a compact structure without visible cracks. However, a distinct diffusion layer is observed. At sintering temperatures of 673 K, 723 K, and 773 K, the thicknesses of the diffusion layer were measured as 1.6 μm, 2.9 μm, and 4.7 μm, respectively, with a sintering time of 5 min. When the sintering time was extended to 10 min at the same temperatures, the thicknesses of the diffusion layer increased to 1.9 μm, 3.5 μm, and 5.0 μm, respectively. Therefore, increasing the sintering temperature and prolonging the sintering time have less effect on the thickness of the diffusion layer. In Fig. 2g, it is evident that the Co content decreases significantly as the diffusion depth increases. The dominant element in the diffusion layer is Te, accompanied by minor quantities of Bi and Sb. Further elemental content analysis reveals that the metallized phase composition consists of Co-8.8 at.%Sb-2.7 at.%Bi-48.3 at.%Te. Based on the literature, this composition corresponds to a ternary alloy

phase known as Co(Sb_{0.15}Te_{0.85})₂, with slight incorporation of Bi doping.^{19,20}

Figure 3 presents the results of the EDS analysis conducted on the Co/Bi_{0.4}Sb_{1.6}Te₃ joint interface produced under the diffusion welding process of 673 K for 5 min. The elements Te, Sb, and Bi are evenly distributed in the Bi_{0.4}Sb_{1.6}Te₃ matrix, while Co is evenly distributed in the Co plating layer. Figure 3d shows that a significant amount of Te accumulates in the reaction layer. This could be due to the stronger affinity of the Co layer towards the Te element, the lower energy required for the combination of Co and Te, and the formation of the Te-rich Co-Sb-Te ternary compound.

The electrical performance of the Co/Bi_{0.4}Sb_{1.6}Te₃ joint interface was assessed by measuring its contact resistivity at three different diffusion welding temperatures of 673 K, 723 K and 773 K, with a diffusion welding time of 5 min. The results show that the Co/Bi_{0.4}Sb_{1.6}Te₃ interface exhibited a low contact resistivity of 0.83 μΩ cm² at both 673 K and 723 K, likely due to the formation of a heterojunction with a matching work function that resulted in an ohmic contact with low resistance.²¹ However, as the reaction temperature increased to 773 K, the thickness of the diffusion-reaction layer increased significantly, resulting in a

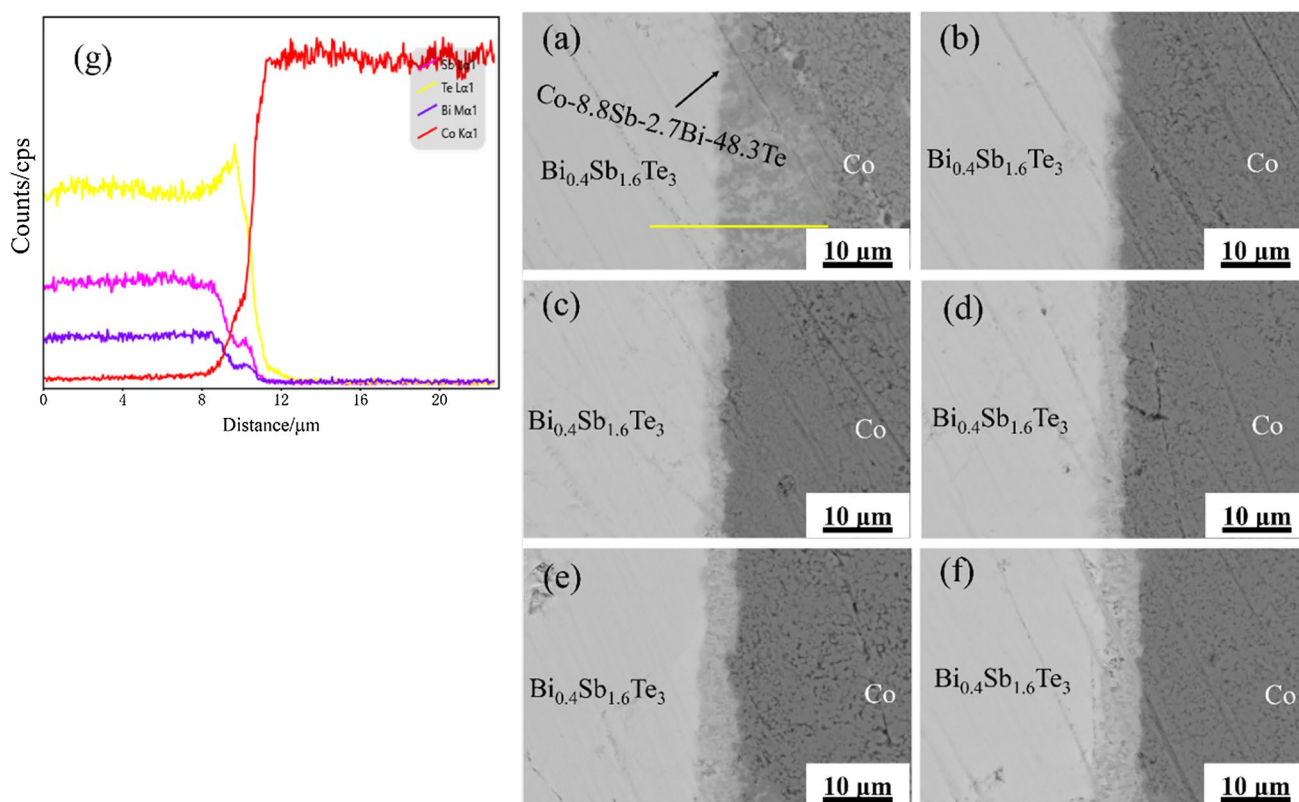


Fig. 2 SEM images of Co/Bi_{0.4}Sb_{1.6}Te₃ joint interface prepared under different diffusion welding processes: (a) 673 K, 5 min; (b) 673 K, 10 min; (c) 723 K, 5 min; (d) 723 K, 10 min; (e) 773 K, 5 min; (f) 773 K, 10 min; (g) EDS diagram at the yellow line in (a) (Color figure online).

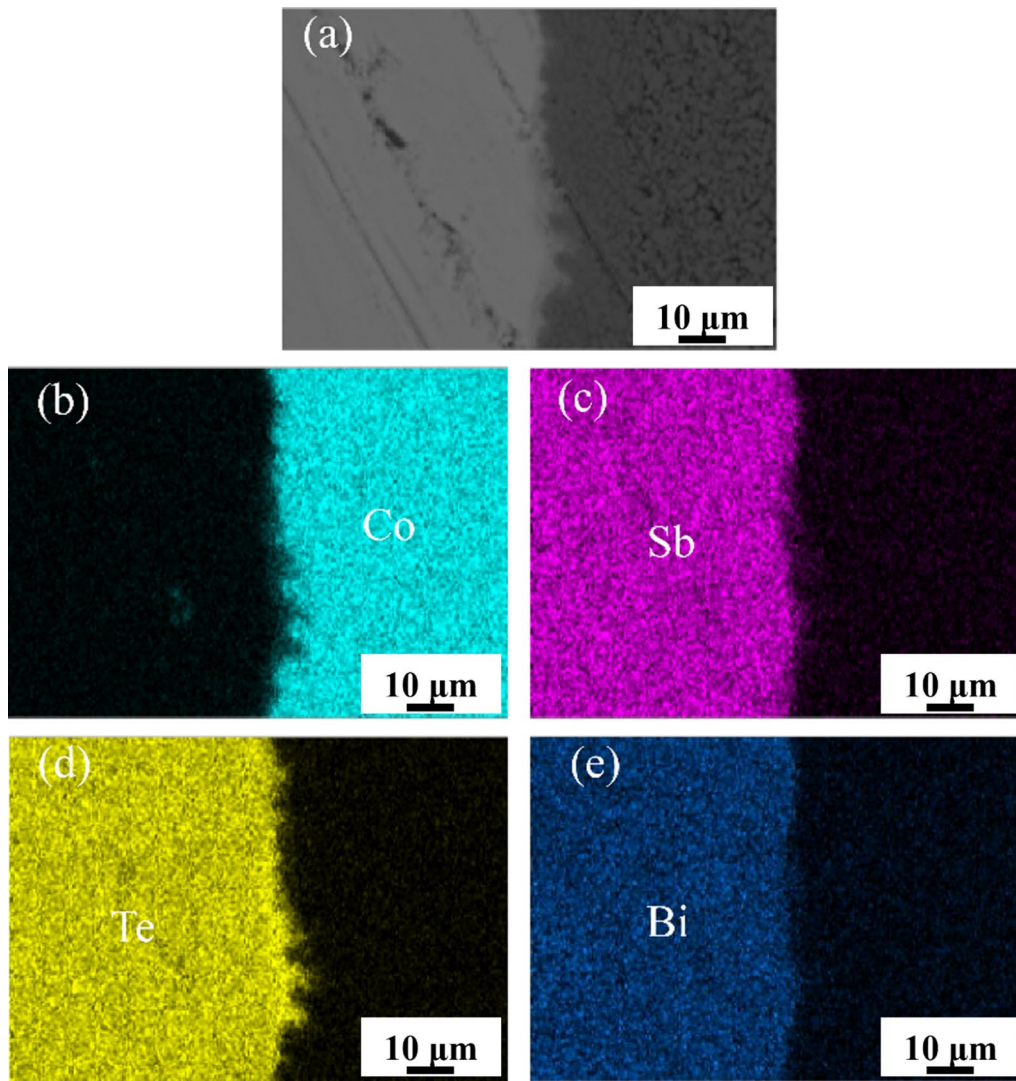


Fig. 3 EDS diagram of elemental distribution at the interface of Co/Bi_{0.4}Sb_{1.6}Te₃ joints prepared at 5 min with diffusion welding at 673 K: (a) SEM image at the joint interface; (b) Co; (c) Sb; (d) Te; (e) Bi.

corresponding increase in resistivity to $7.33 \mu\Omega \text{ cm}^2$. This is likely because the increased thickness of the diffusion-reaction layer caused an increase in contact resistance.

Figure 4 illustrates the interfacial bonding strength of the Co/Bi_{0.4}Sb_{1.6}Te₃ joint under various process conditions. At a sintering time of 5 min, the interfacial bonding strength of the Co/Bi_{0.4}Sb_{1.6}Te₃ joint increased from 4.86 MPa at 673 K to 5.17 MPa at 773 K as the sintering temperature rose, representing a 6.4% improvement. When the sintering time was extended to 10 min, the maximum enhancement in interfacial bonding strength was 1.2%. This observation indicates that the interfacial bonding strength is more strongly influenced by the sintering temperature than the sintering time.

The SEM and EDS results presented in Fig. 5 illustrate the Co/Bi₂Te_{2.7}Se_{0.3} joints prepared under various diffusion welding conditions. The findings indicate a tightly

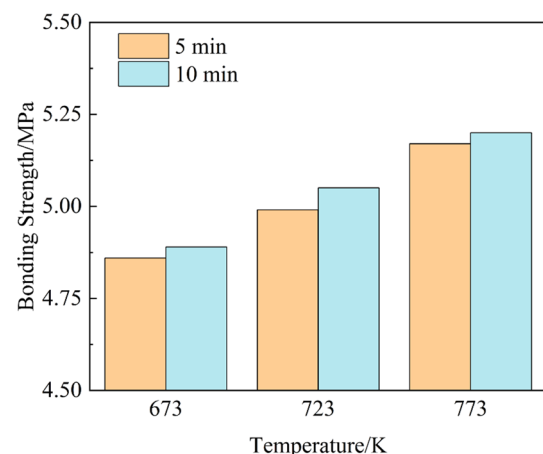


Fig. 4 Bonding strength of Co/Bi_{0.4}Sb_{1.6}Te₃ joint prepared under different diffusion welding processes.

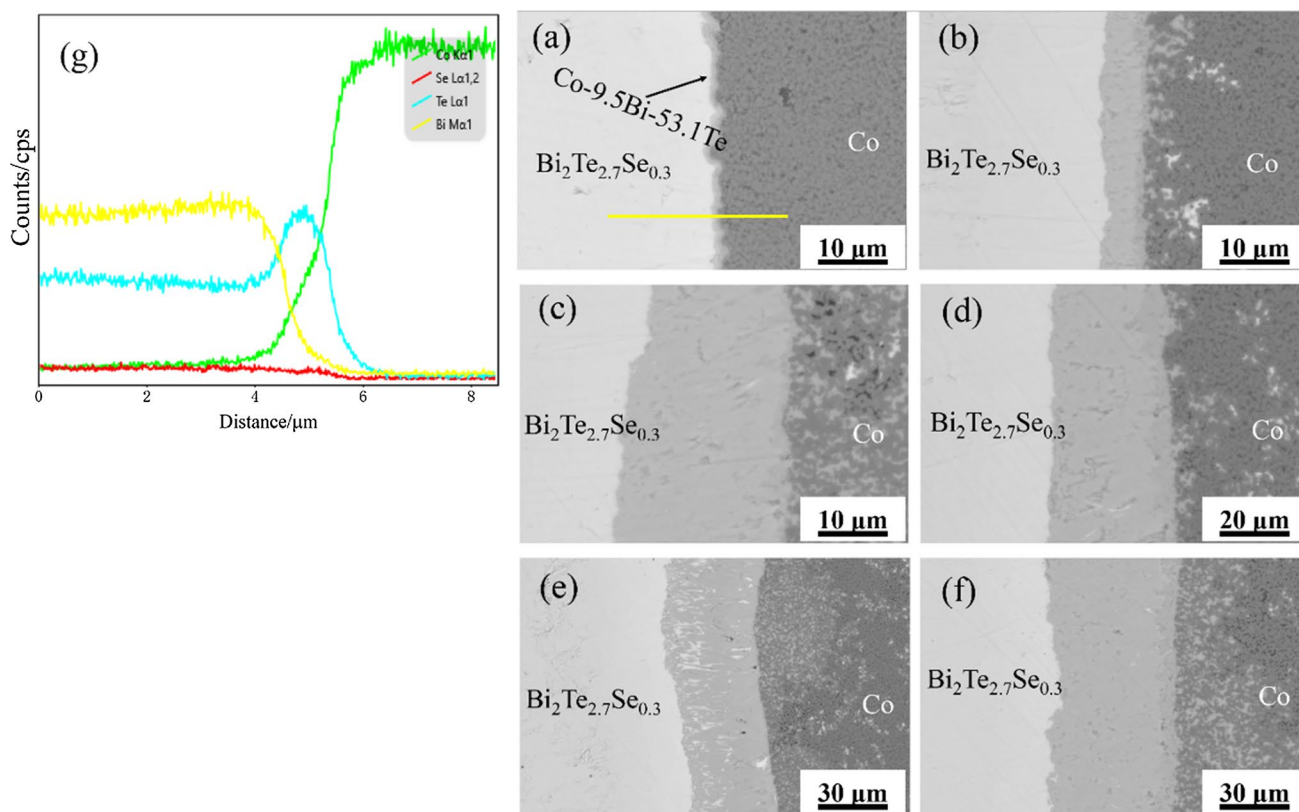


Fig. 5 SEM images of $\text{Co}/\text{Bi}_2\text{Te}_{2.7}\text{Se}_{0.3}$ interface prepared under different diffusion welding processes: (a) 673 K, 5 min; (b) 673 K, 10 min; (c) 723 K, 5 min; (d) 723 K, 10 min; (e) 773 K, 5 min; (f) 773 K, 10 min; (g) EDS diagram at the yellow line in (a) (Color figure online).

bonded interface between the Co coating and $\text{Bi}_2\text{Te}_{2.7}\text{Se}_{0.3}$ without any visible cracks, but with the formation of a substantial diffusion layer. The thickness of the diffusion layer was measured as 1.6 μm , 23.1 μm , and 36.4 μm at sintering temperatures of 673 K, 723 K, and 773 K, respectively, with a sintering time of 5 min. When the sintering time was extended to 10 min at the same temperatures, the thickness of the diffusion layer increased to 5.9 μm , 35.6 μm , and 65.4 μm , respectively. Thus, increasing the sintering temperature and prolonging the sintering time significantly affect the thickness of the diffusion layer, which contradicts the observations in the case of $p\text{-Bi}_2\text{Te}_3$. This difference may be attributed to the variations in their composition. Xiong et al. investigated the formation energy between Co and bismuth telluride by first-principles calculations, and found that the formation energy of Co with Te is higher than that of Co with Bi .²² Consequently, based on the principle of lowest energy, the higher the Bi content, the more stable the compound formed by Co with bismuth telluride. This explains why the interfacial reaction layer of $n\text{-Bi}_2\text{Te}_3$ with Co is thicker than $p\text{-Bi}_2\text{Te}_3$. Additionally, higher temperatures provide a stronger diffusion driving force, further promoting element diffusion.²³ The combined effect of these factors makes the $\text{Co}/\text{Bi}_2\text{Te}_{2.7}\text{Se}_{0.3}$ joint interface more sensitive to

variations in sintering temperature and time. EDS analysis in Fig. 5g indicates that the diffusion layer consists of approximately 9.5 at.% Co , 53.1 at.% Te , and 48.3 at.% Bi , which likely corresponds to a Bi -doped CoTe_2 binary alloy phase.²⁴

To further analyze the elemental distribution of the interface layer, EDS analysis was performed on the $\text{Co}/\text{Bi}_2\text{Te}_{2.7}\text{Se}_{0.3}$ joint interface prepared under the diffusion welding process with a temperature of 673 K and a duration of 5 min. The results of this analysis are depicted in Fig. 6. As illustrated in Fig. 6d and e, it is evident that the Te element is concentrated in the diffusion reaction layer, while the Bi element is slightly enriched at the edge of the $\text{Bi}_2\text{Te}_{2.7}\text{Se}_{0.3}$ matrix material. This can be attributed to the fact that during the diffusion welding process, the Co element in the Co layer diffused into the $\text{Bi}_2\text{Te}_{2.7}\text{Se}_{0.3}$ base material, resulting in a solid solution that formed at the $\text{Co}/\text{Bi}_2\text{Te}_{2.7}\text{Se}_{0.3}$ interface. This is likely because the combination of Co and Te requires the lowest binding energy, thus easily forming CoTe_2 compounds.¹⁸ The Te on the left side of the diffusion layer is pulled towards the Co layer, causing the relative enrichment of missing Bi in Te .

The contact resistivity of the $\text{Co}/\text{Bi}_2\text{Te}_{2.7}\text{Se}_{0.3}$ joint interface was tested for three different diffusion welding temperatures of 673 K, 723 K and 773 K, with a diffusion welding

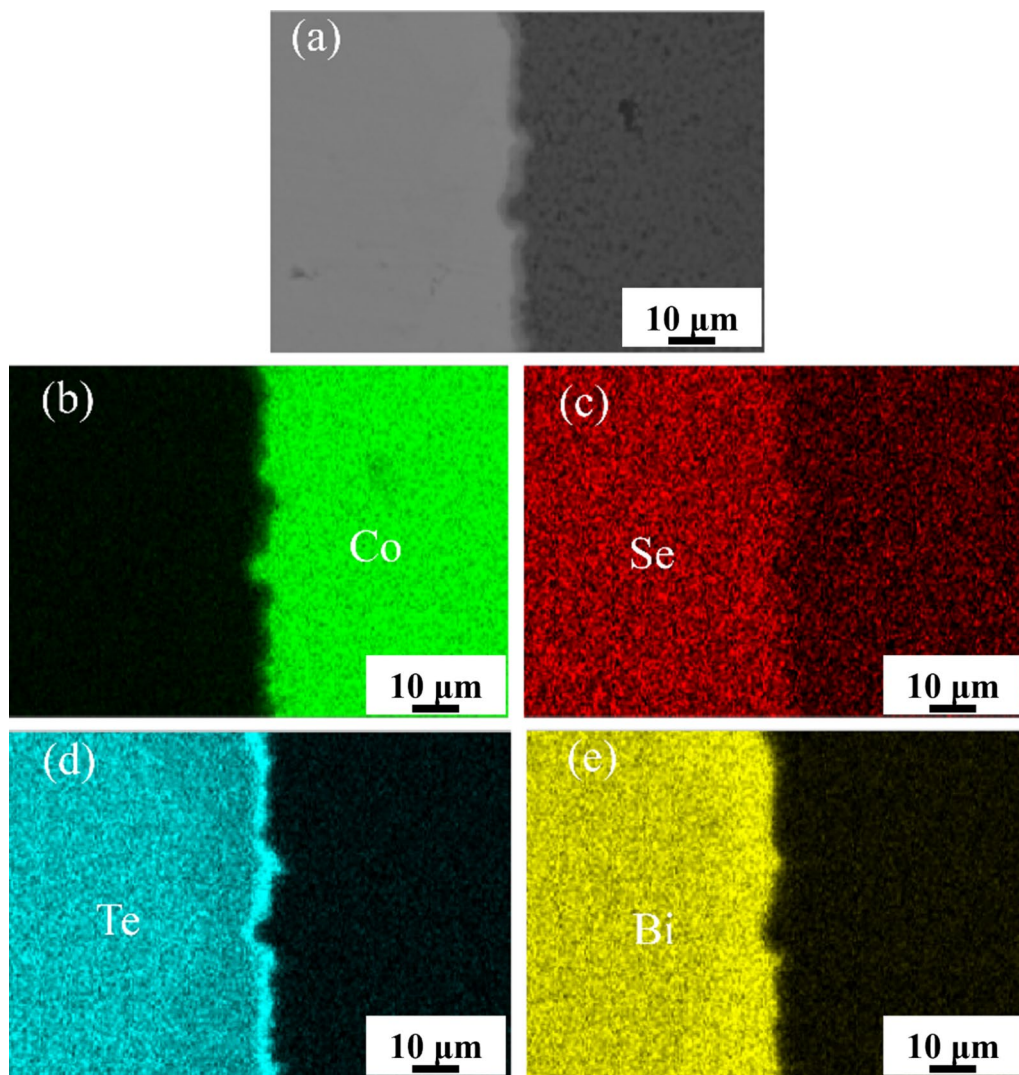


Fig. 6 EDS diagram of elemental distribution at the interface of Co/Bi₂Te_{2.7}Se_{0.3} joints prepared under 5 min with diffusion welding at 673 K: (a) SEM image at the joint interface; (b) Co; (c) Se; (d) Te; (e) Bi.

time of 5 min. The results demonstrate that the interface of the Co/Bi₂Te_{2.7}Se_{0.3} joint presents a low contact resistivity at low temperatures, with a value of 0.75 $\mu\Omega\text{ cm}^2$ at 673 K. This phenomenon is consistent with the Co/Bi_{0.4}Sb_{1.6}Te₃ interface and can be attributed to the formation of a low-resistance metal compound layer. As the reaction temperature increases, the contact resistance of the Co/Bi₂Te_{2.7}Se_{0.3} interface increases dramatically, reaching 4.51 $\mu\Omega\text{ cm}^2$ and 10.18 $\mu\Omega\text{ cm}^2$ at 723 K and 773 K, respectively.

Figure 7 presents the interfacial bonding strength of Co/Bi₂Te_{2.7}Se_{0.3} joints under different processing conditions. The results demonstrate a general trend of increasing and then decreasing interfacial bonding strength with increasing sintering temperature and sintering time. This behavior may be attributed to the rapid growth of the diffusion layer thickness. Initially, as the thickness of the diffusion layer

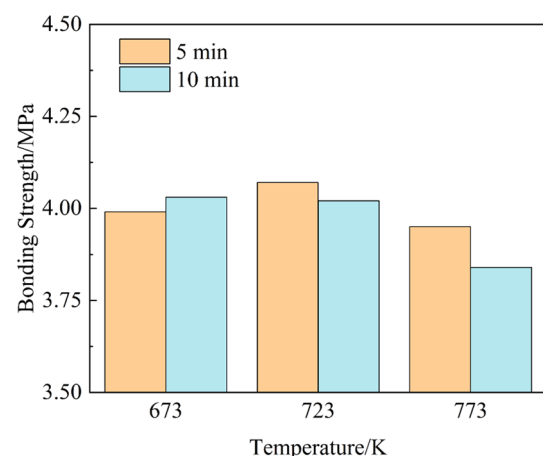


Fig. 7 Bonding strength of Co/Bi₂Te_{2.7}Se_{0.3} joints prepared using different diffusion welding processes.

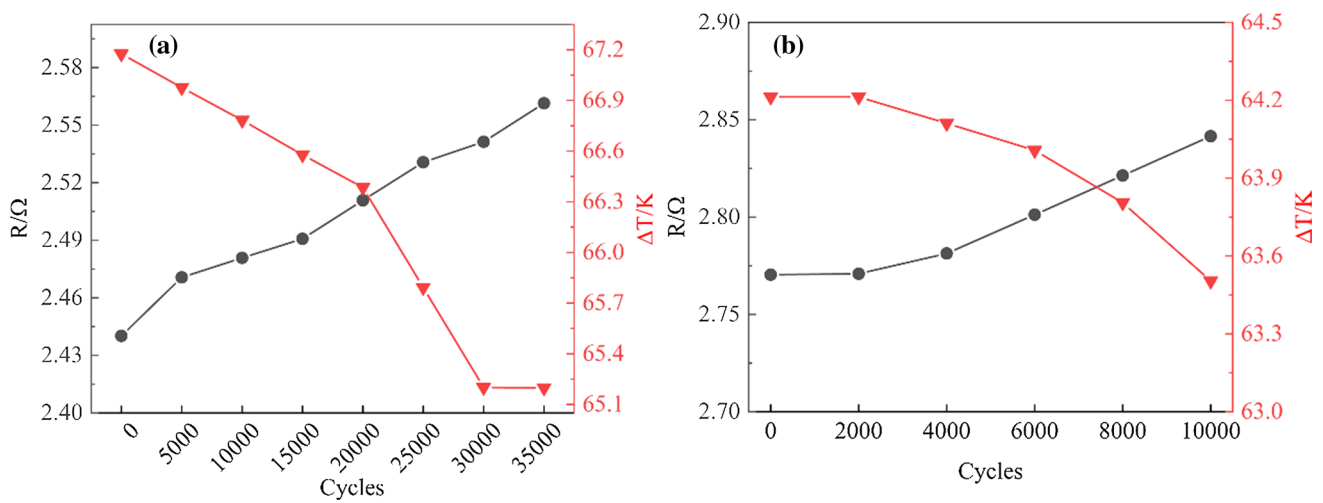


Fig. 8 Change in service performance of (a) Co barrier layer and (b) Ni barrier layer devices.

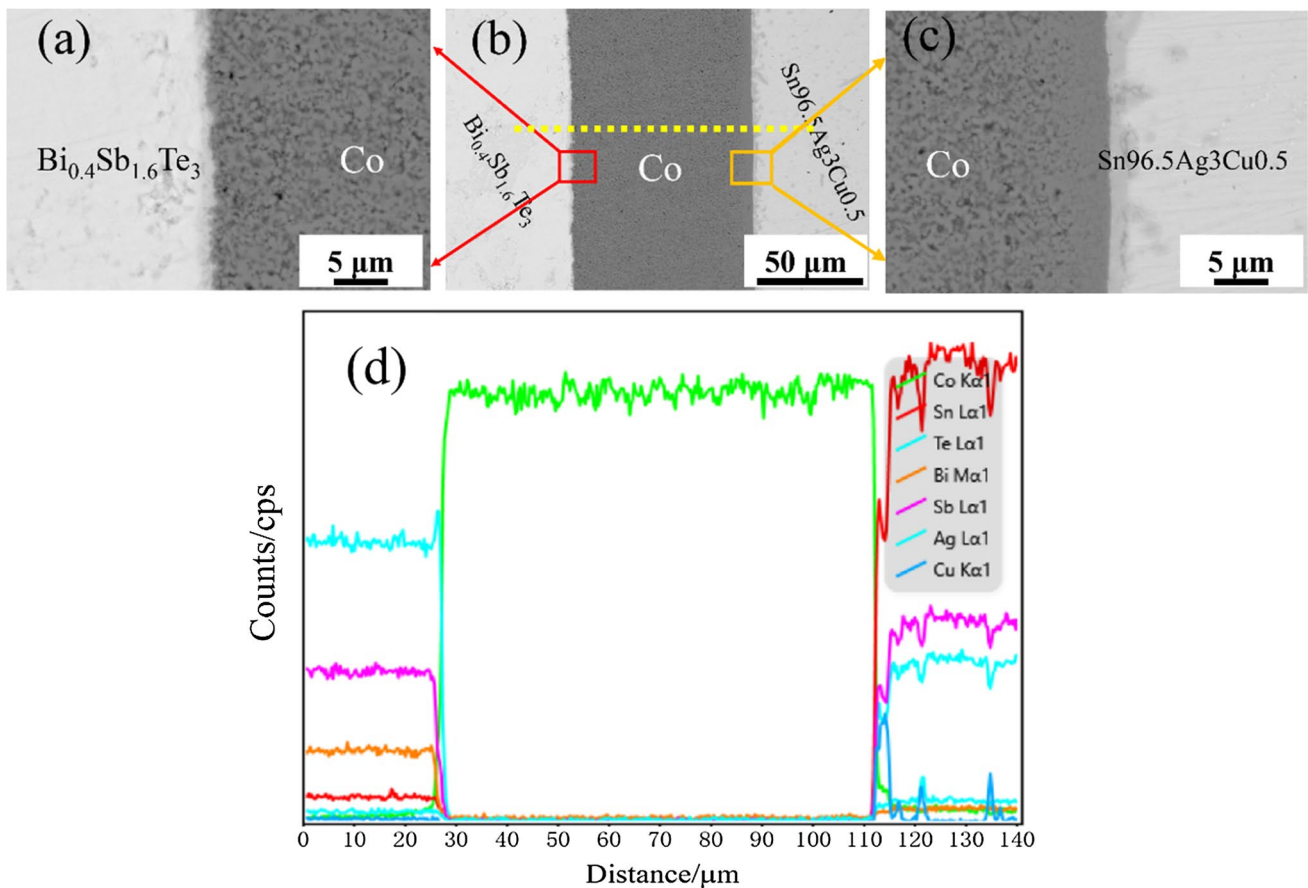


Fig. 9 SEM images of the (a) $\text{Bi}_{0.4}\text{Sb}_{1.6}\text{Te}_3/\text{Co}$, (b) $\text{Bi}_{0.4}\text{Sb}_{1.6}\text{Te}_3/\text{Co}/\text{Sn}_{96.5}\text{Ag}_3\text{Cu}_{0.5}$, and (c) $\text{Co}/\text{Sn}_{96.5}\text{Ag}_3\text{Cu}_{0.5}$ interface after service; (d) EDS diagram at the dotted line.

increases, the bonding between the Co layer and the bismuth telluride substrate becomes stronger. This leads to an increase in the interfacial bonding strength. However, with the increasing thickness of the diffusion layer, the interfacial

bonding strength starts to decrease due to the poor mechanical properties of the compound CoTe_2 formed in the diffusion layer.

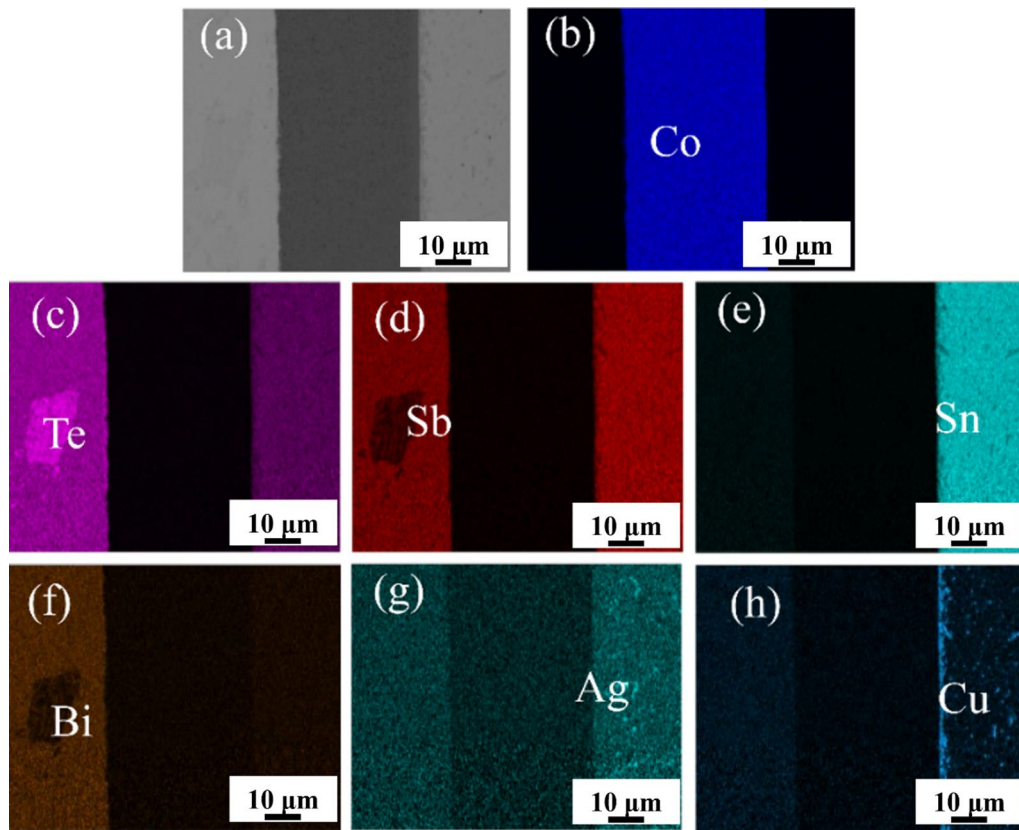


Fig. 10 EDS diagram of elemental distribution at the interface of $\text{Bi}_{0.4}\text{Sb}_{1.6}\text{Te}_3/\text{Co}/\text{Sn}_{96.5}\text{Ag}_3\text{Cu}_{0.5}$ after service: (a) SEM image at the joint interface; (b) Co; (c) Te; (d) Sb; (e) Sn; (f) Bi; (g) Ag; (h) Cu.

The performance of thermoelectric devices with Co and Ni as barrier layer materials was evaluated through a 10–90 alternating current shock test. Figure 8 displays the changes in the performance of the devices during the test. The results indicate that the internal resistance of the thermoelectric device with Co as the barrier layer increases with the number of cycles, and after 35,000 cycles, the increase in resistance exceeds 5% of the initial resistance value, making the device fail according to GR-468. The temperature difference (ΔT) of the device also decreases with the increase in cycles; however, the decrease is gradual before 20,000 cycles, suggesting that the Co-plating diffusion welding process has excellent barrier properties. The service life of the device with Co as the barrier layer is significantly longer than that of the Ni barrier layer device, thereby highlighting Co's suitability as an outstanding barrier material.

Figure 9 presents the SEM and EDS results of $\text{Bi}_{0.4}\text{Sb}_{1.6}\text{Te}_3/\text{Co}/\text{Sn}_{96.5}\text{Ag}_3\text{Cu}_{0.5}$ after service testing. As shown in Fig. 9a, the contact between the $\text{Co}/\text{Bi}_{0.4}\text{Sb}_{1.6}\text{Te}_3$ is found to be intact without any visible cracks. Moreover, the thickness of the diffusion layer remains mostly unchanged, suggesting that the reaction between Co and the bismuth telluride matrix occurs at a slow rate. EDS analysis reveals

that the diffusion layer consists primarily of Te, Sb, and Co, while no elements from the solder are detected. This indicates that the Co barrier layer effectively hinders the diffusion of solder elements into the bismuth telluride matrix. Figure 9c illustrates the formation of a distinct metal compound layer between the solder and the Co layer. The EDS results demonstrate a high concentration of Cu in this compound layer, indicating the aggregation of Cu elements from the solder at the $\text{Co}/\text{Sn}_{96.5}\text{Ag}_3\text{Cu}_{0.5}$ interface during service. Additionally, some Te and Sb elements diffuse from the bismuth telluride matrix into the interior of the solder. This behavior might be attributed to the higher melting point of Co compared to 1673 K. Consequently, the Co layer cannot fully densify at the sintering temperature of 673 K, leading to the formation of voids that serve as channels for the diffusion of Te elements.

The results of the EDS analysis of the post-service interface of the solder/ $\text{Co}/\text{Bi}_{0.4}\text{Sb}_{1.6}\text{Te}_3$ particle component are shown in Fig. 10. The analysis reveals that the Co barrier layer provides a clear barrier to elements Sn, Bi, and Cu, but its effect on the diffusion of Te and Sb elements from the $\text{Bi}_{0.4}\text{Sb}_{1.6}\text{Te}_3$ into the solder is relatively weak, which is identified as a key factor contributing to the device failure.

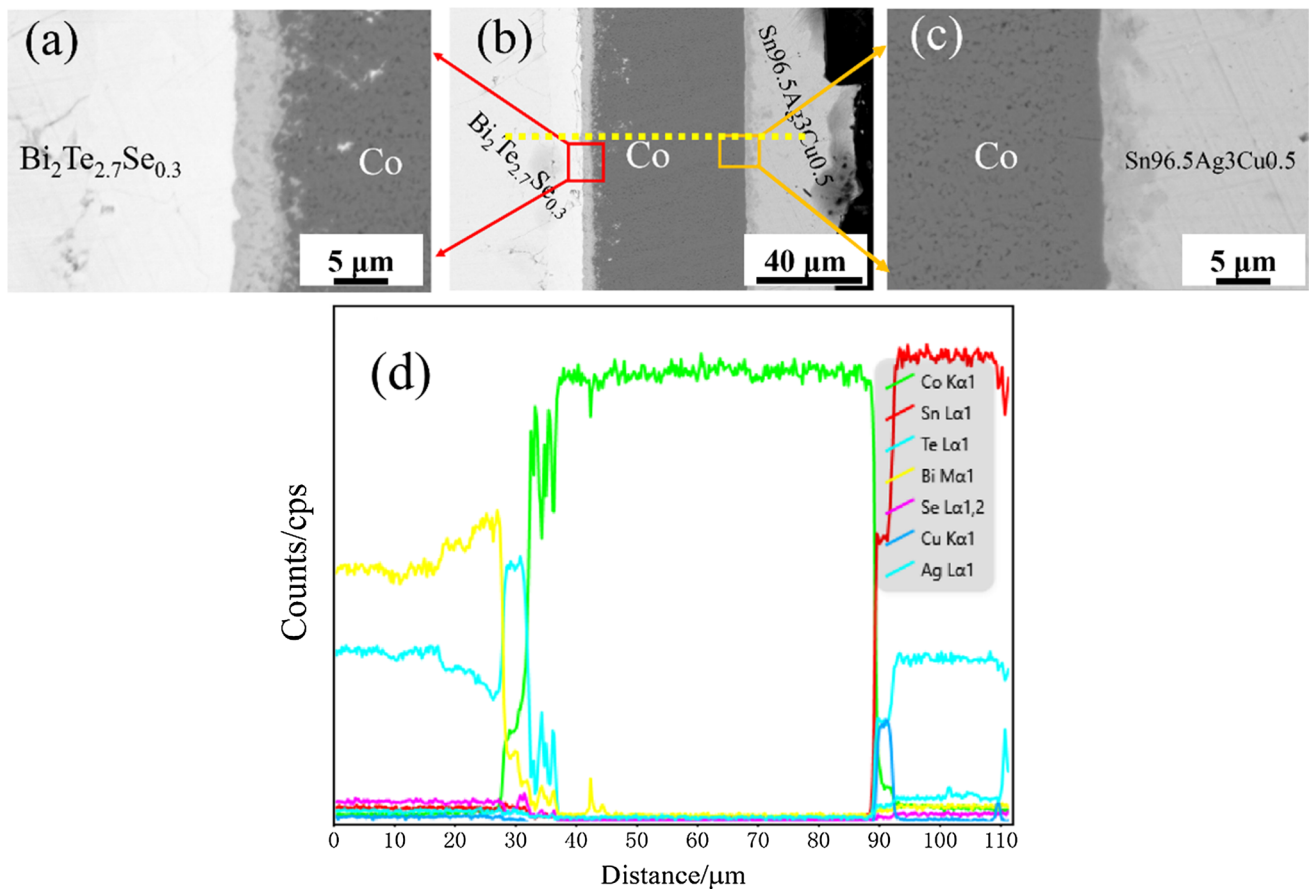


Fig. 11 SEM images of the (a) $\text{Bi}_2\text{Te}_{2.7}\text{Se}_{0.3}/\text{Co}$, (b) $\text{Bi}_2\text{Te}_{2.7}\text{Se}_{0.3}/\text{Co}/\text{Sn}_{96.5}\text{Ag}_3\text{Cu}_{0.5}$, and (c) $\text{Co}/\text{Sn}_{96.5}\text{Ag}_3\text{Cu}_{0.5}$ interface after service; (d) EDS diagram at the dotted line.

Figure 11 shows the SEM and EDS results of the $\text{Bi}_2\text{Te}_{2.7}\text{Se}_{0.3}/\text{Co}/\text{Sn}_{96.5}\text{Ag}_3\text{Cu}_{0.5}$ system after service. From Fig. 11a, it can be observed that there is a good contact between $\text{Co}/\text{Bi}_2\text{Te}_{2.7}\text{Se}_{0.3}$ without any obvious cracks. However, an obvious elemental diffusion phenomenon is visible, and combined with the EDS results, it shows that the diffusion layer mainly contains Bi, Te, and Co. No elements from the solder are found, indicating that the Co barrier layer can effectively block the diffusion of elements from solder into the bismuth telluride substrate during the service process. It can be observed from Fig. 11c that an obvious metal compound layer is formed between $\text{Co}/\text{Sn}_{96.5}\text{Ag}_3\text{Cu}_{0.5}$. The EDS results show that the compound layer is enriched with Cu, indicating that the Cu in the solder will be aggregated at the $\text{Co}/\text{Sn}_{96.5}\text{Ag}_3\text{Cu}_{0.5}$ interface during the service process. Concomitantly, noteworthy diffusion of Te elements from the bismuth telluride matrix into the solder interior is discernible, likely attributable to the higher melting point of Co exceeding 1673 K. Therefore, it is not possible to fully densify the Co layer at the sintering temperature of

673 K. These voids provide a channel for the diffusion of Te elements.

A detailed analysis of the diffusion behavior of elements was conducted by performing EDS analysis on the service-aged solder/ $\text{Co}/\text{Bi}_2\text{Te}_{2.7}\text{Se}_{0.3}$ interface, as illustrated in Fig. 12. The results, as shown in Fig. 12c and d, reveal that Te was concentrated at the $\text{Co}/\text{Bi}_2\text{Te}_{2.7}\text{Se}_{0.3}$ interface due to its attraction to Co in the diffusion reaction layer, while Bi was hindered and enriched in the barrier layer.

The results of the EDS analysis shown in Fig. 12 reveal that the Co barrier layer has a clear barrier effect on the elements Sn, Bi, and Cu, as demonstrated by the enrichment of these elements at the interface of the solder/Co. However, the barrier effect of the Co layer on the diffusion of Te elements from the $\text{Bi}_2\text{Te}_{2.7}\text{Se}_{0.3}$ into the solder is relatively weak, as evidenced by the enrichment of Te at the $\text{Co}/\text{Bi}_2\text{Te}_{2.7}\text{Se}_{0.3}$ interface and its attraction towards Co in the diffusion reaction layer. This weakness in the barrier effect of the Co layer is identified as one of the primary reasons for device failure.

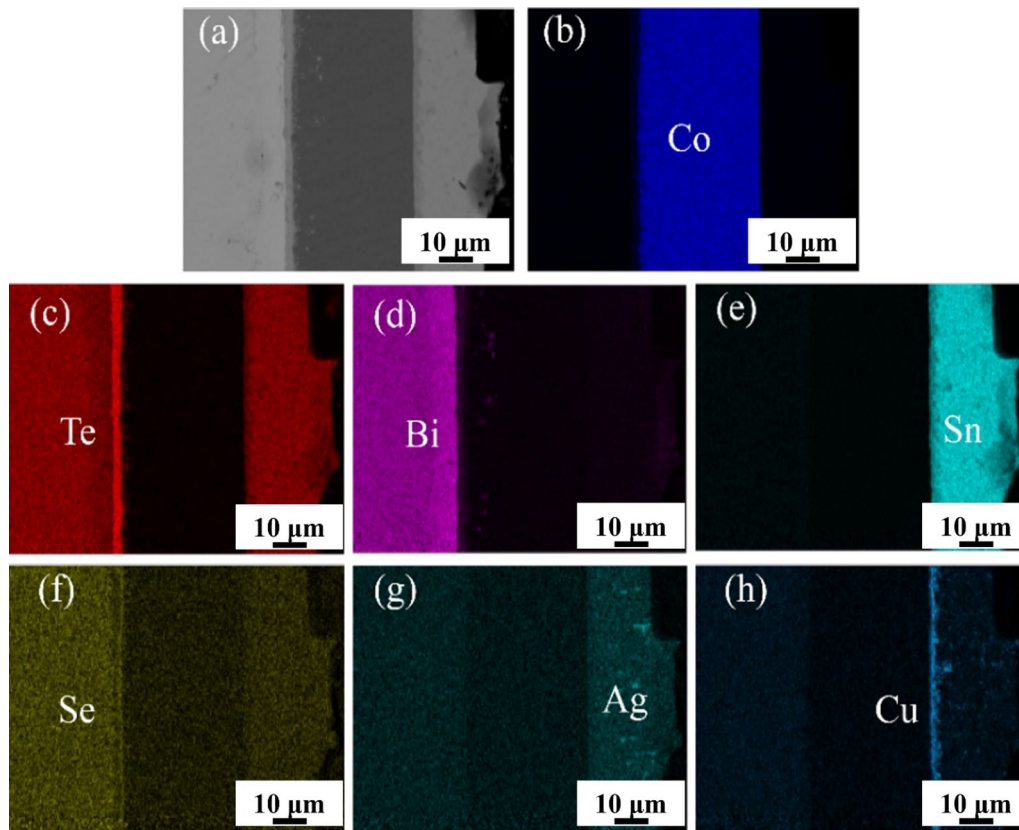


Fig. 12 EDS diagram of elemental distribution at the interface of $\text{Bi}_2\text{Te}_{2.7}\text{Se}_{0.3}/\text{Co}/\text{Sn}_{96.5}\text{Ag}_3\text{Cu}_{0.5}$ after service: (a) SEM image at the joint interface; (b) Co; (c) Te; (d) Bi; (e) Sn; (f) Se; (g) Ag; (h) Cu.

Conclusions

In this study, the authors examine the diffusion and connection effects of $\text{Co}/\text{Bi}_{0.4}\text{Sb}_{1.6}\text{Te}_3$ and $\text{Co}/\text{Bi}_2\text{Te}_{2.7}\text{Se}_{0.3}$ joints under various diffusion welding conditions. The focus of the research is on evaluating the performance of thermoelectric devices with a Co-plated barrier layer that are produced through diffusion welding. The results show that the thickness of the diffusion layer at the $\text{Co}/\text{Bi}_{0.4}\text{Sb}_{1.6}\text{Te}_3$ interface increases with the temperature and duration of the diffusion welding process, although the degree of diffusion is low and the maximum thickness does not exceed $6 \mu\text{m}$. The contact resistance at the interface also increases with the temperature, while the hardness of the Co barrier layer increases with both temperature and duration. Based on these findings, the authors conclude that a temperature of 673 K and a duration of 5 min is the optimal process for preparing the Co barrier layer for the $\text{Bi}_{0.4}\text{Sb}_{1.6}\text{Te}_3$. Similar results are found for the $\text{Co}/\text{Bi}_2\text{Te}_{2.7}\text{Se}_{0.3}$ joints, with the authors recommending the same diffusion welding conditions for the $\text{Bi}_2\text{Te}_{2.7}\text{Se}_{0.3}$. The authors also show that thermoelectric devices produced

through this diffusion welding and plating process exhibit a cycle number of over 35,000 before failure, significantly outperforming devices produced with Ni as the barrier layer material. This study highlights the excellent barrier effects of Co on elements such as Cu, Sn, and Bi, leading to improved performance of thermoelectric devices in service.

Acknowledgments This work was supported by the Enterprise Technological Innovation and Development Project Supported by Hubei Province (QYJSCX2021000321), the Ministry of Science and Technology's Key Project of "Science and Technology help Economy 2020" (SQ2020YFF0404755), the Science and Technology Program of Ezhou City (EZ01-001-20190001) and the "Innovation and Entrepreneurship Strategic Team" Project of Hubei Province (CYTDC2018000094).

Author contributions SJ: Conceptualization, Data curation, Investigation, Methodology, Resources, Software, Writing—original draft. ZK: Formal analysis, Validation. XH: Writing—review & editing. XC: Resources, Validation. FZ: Investigation. XF: Funding acquisition, Project administration, Supervision.

Conflict of interest The authors declare that they have no known competing financial interests or personal relationships that could have appeared to influence the work reported in this paper.

References

1. Y. Cao, X. Zhao, T. Zhu, X. Zhang, and J. Tu, Syntheses and thermoelectric properties of Bi₂Te₃/Sb₂Te₃ bulk nanocomposites with laminated nanostructure. *Appl. Phys. Lett.* 92, 143106 (2008).
2. X. Ji, J. He, Z. Su, N. Gothard, and T. Tritt, Improved thermoelectric performance in polycrystalline *p*-type Bi₂Te₃ via an alkali metal salt hydrothermal nanocoating treatment approach. *J. Appl. Phys.* 104(3), 034907 (2008).
3. J. Sootsman, D. Chung, and M. Kanatzidis, New and old concepts in thermoelectric materials. *Angew. Chem. Int. Ed.* 48(46), 8616 (2009).
4. H. Wu, M. Kaviani, and O. Kwon, Thermophotovoltaic power conversion using a superadiabatic radiant burner. *Appl. Energy* 209, 392 (2018).
5. F. Yu, S. Chen, W. Liu, J. Li, and B. Wan, Research status and development trend of Bi₂Te₃ thermoelectric materials. *J. Yanshan Univ.* 41(3), 20 (2017).
6. H. Zhou, M. Tan, J. Zhang, X. Niu, R. Wang, and G. Pan, Research status of Bi₂Te₃ thermoelectric materials. *Semicond. Technol.* 36(10), 765 (2011).
7. J. Zhang, Thermoelectric Technology. (Tianjin Science and Technology Press, Tianjin, 2013), p. 131, 219.
8. S. Park, Y. Kim, H. Jang, C. Hwang, J. Choi, I. Lee, and M. Oh, Fe-Ni-Cr diffusion barrier for high-temperature operation of Bi₂Te₃. *J. Alloy. Compd.* 932, 167537 (2023).
9. E. Hatzikraniotis, K. Zorbas, I. Samaras, T. Kyratsi, and K. Paraskevopoulos, Efficiency study of a commercial thermoelectric power generator (TEG) under thermal cycling. *J. Electron. Mater.* 39(9), 2112 (2010).
10. M. Barako, W. Park, A. Marconnet, M. Asheghi, and K. Goodson, Thermal cycling, mechanical degradation, and the effective figure of merit of a thermoelectric module. *J. Electron. Mater.* 42, 372 (2013).
11. Y. Nguyen and I. Son, Thermomechanical stability of Bi₂Te₃-based thermoelectric modules employing variant diffusion barriers. *Intermetallics* 140, 107404 (2022).
12. W. Liu, H. Wang, L. Wang, X. Wang, G. Joshi, G. Chen, and Z. Ren, Understanding of the contact of nanostructured thermoelectric *n*-type Bi₂Te_{2.7}Se_{0.3} legs for power generation applications. *J. Mater. Chem. A* 1, 13093 (2013).
13. T. Shi, J. Zheng, X. Wang, P. Zhang, P. Zong, and K. Razeeb, Recent advances of electrodeposition of Bi₂Te₃ and its thermoelectric applications in miniaturized power generation and cooling. *Int. Mater. Rev.* 68, 521 (2022).
14. T. Clin, S. Turenne, D. Vasilevskiy, and R. Masut, Numerical simulation of the thermomechanical behavior of extruded bismuth telluride alloy module. *J. Electron. Mater.* 38(7), 994 (2009).
15. H. Kim, T. Wang, W. Liu, and Z. Ren, Engineering thermal conductivity for balancing between reliability and performance of bulk thermoelectric generators. *Adv. Func. Mater.* 26(21), 3678 (2016).
16. W. Liu, H. Wang, L. Wang, X. Wang, G. Joshi, G. Chen, and Z. Ren, Understanding of the contact of nanostructured thermoelectric *n*-type Bi₂Te_{2.7}Se_{0.3} legs for power generation applications. *J. Mater. Chem. A* 1(42), 3678 (2013).
17. H. Hsieh, C. Wang, W. Lin, S. Chakraborty, T. Lee, H. Chu, and A. Wu, Electroless Co-P diffusion barrier for *n*-PbTe thermoelectric material. *J. Alloy. Compd.* 728, 1023 (2017).
18. C. Wang, H. Hsieh, Z. Sun, V. Ranganayakulu, T. Lan, Y. Chen, Y. Chang, and A. Wu, Interfacial stability in Bi₂Te₃ thermoelectric joints. *ACS Appl. Mater. Interfaces* 12(24), 27001 (2020).
19. G. Yamaguchi, M. Shimada, and M. Koizumi, Preparation and crystal structure of Fe(Sb_{1-x}Te_x)₂ and Co(Sb_{1-x}Te_x)₂ (0 ≤ x ≤ 1.0). *J. Solid State Chem.* 19(1), 63 (1976).
20. P. Terzieff and H. Ipser, A contribution to the ternary phase diagram Co-Sb-Te. *Monatshefte für Chemie-Chem. Mon.* 123(1), 35 (1992).
21. Y. Liu, Effect of annealing temperature on properties of Co-sputtered Bi₂Te₃. *Mater. Sci. Eng.* 782, 022041 (2020).
22. K. Xiong, W. Wang, H. Alshareef, R. Gupta, J. White, B. Gnade, and K. Cho, Electronic structures and stability of Ni/Bi₂Te₃ and Co/Bi₂Te₃ interfaces. *J. Phys. D Appl. Phys.* 43, 115303 (2010).
23. Q. Yang, B. Meng, Z. Lin, X. Zhu, F. Yang, and S. Wu, Effect of sintering temperature on the elemental diffusion and electrical conductivity of SrTiO₃/YSZ composite ceramic. *Ionics* 23, 967 (2017).
24. C. Crawford, B. Ortiz, P. Gorai, V. Stevanovic, and E. Toberer, Experimental and computational phase boundary mapping of Co₄Sn₆Te₆. *J. Mater. Chem. A* 6, 24175 (2018).

Publisher's Note Springer Nature remains neutral with regard to jurisdictional claims in published maps and institutional affiliations.

Springer Nature or its licensor (e.g. a society or other partner) holds exclusive rights to this article under a publishing agreement with the author(s) or other rightsholder(s); author self-archiving of the accepted manuscript version of this article is solely governed by the terms of such publishing agreement and applicable law.